

Fission Experiments with Secondary Beams

K.-H. Schmidt^a, S. Steinhäuser^b, C. Böckstiegel^b, A. Grewe^b,
J. Benlliure^a, H.-G. Clerc^b, A. Heinz^a, M. de Jong^b,
A. R. Junghans^a, J. Müller^b, M. Pfützner^c

^a*Gesellschaft für Schwerionenforschung m. b. H., Planckstraße 1, 64291 Darmstadt, Germany*

^b*Institut für Kernphysik, Technische Universität Darmstadt,
Schloßgartenstraße 9, 64289 Darmstadt, Germany*

^c*Institute of Experimental Physics, University of Warsaw,
Ul Hoza 69, 00-381 Warszawa, Poland*

Abstract. Nuclear fission from excitation energies around 11 MeV was studied at GSI Darmstadt for 76 neutron-deficient actinides and pre-actinides by use of relativistic secondary beams. The characteristics of multimodal fission of nuclei around ²²⁶Th are systematically investigated and related to the influence of shell effects on the potential-energy and on the level density between saddle point and scission. A systematic view on the large number of elemental yields measured gave rise to a new interpretation of the enhanced production of even elements in nuclear fission and allowed for a new understanding of pair breaking in fission.

INTRODUCTION

Nuclear fission provides unique information on the reordering of nucleons in a large-scale collective motion. The signatures of shell structure and pairing correlations show up in fission from low excitation energies. They have general implications on the influence of shell structure on nuclear dynamics and on the viscosity of cold nuclear matter. The use of secondary beams gives access to a large new field of fissioning systems by overcoming restrictions of conventional experimental techniques.

In this contribution, the large body of data acquired in a recent experiment is presented and the resulting progress in the understanding of the fission dynamics is sketched.

EXPERIMENT

The secondary-beam facility of GSI Darmstadt offers unique possibilities to provide secondary beams of neutron-deficient actinides and preactinides produced by fragmentation of relativistic ²³⁸U projectiles. Within the limits given by the primary-beam intensity and the fragmentation cross sections (1,2), nuclear charge and mass number of the secondary projectiles can freely be selected by tuning the fragment separator (3).

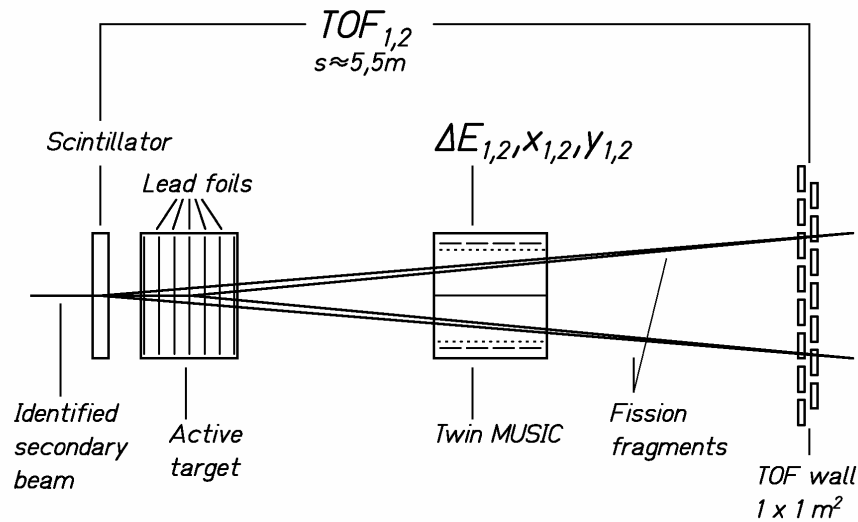


Figure 1. Schematical drawing of the set up for the fission experiment mounted behind the fragment separator

Fission from the desired excitation-energy range slightly above the fission barrier was induced by electromagnetic interactions in a heavy target material. In the next chapter we give a detailed description of this excitation mechanism.

The experimental setup behind the fragment separator is sketched in Figure 1. As secondary target we used a stack of lead foils with a total thickness of 3 g/cm^2 mounted in a gas-filled chamber which acts as a subdivided ionization chamber (active target). With this device it is possible to discriminate fission induced in the lead foils against fission induced in other layers, e.g. the scintillator. The average energy of the secondary projectiles in the lead target was about 430 A MeV . The differential energy loss of each fission fragment was measured separately with an horizontally subdivided twin

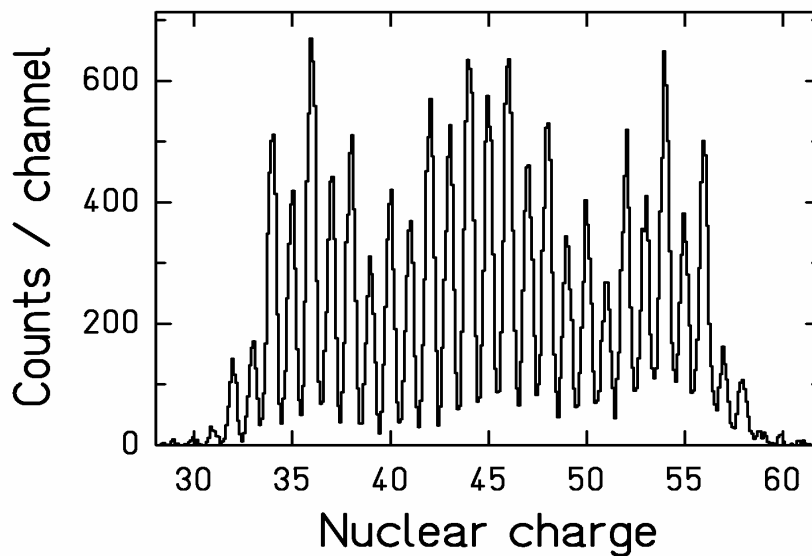


Figure 2. Nuclear-charge response of the twin MUSIC with velocity correction applied as obtained for the fission fragments after electromagnetic excitation of ^{226}Th projectiles.

ionization chamber. In order to correct the energy loss for the velocity dependence, the time-of-flight of the fission fragments was measured by means of a (1m×1m) scintillator wall.

Figure 2 shows the nuclear-charge response of the experimental set up for fission fragments after electromagnetic-induced fission of ^{226}Th . Due to the high center-of-mass energies, an excellent charge resolution is achieved. Events stemming from reactions at lower impact parameters with nuclear contact were suppressed. For details of the analysis procedure see refs. (4,5).

EXCITATION MECHANISM

The electromagnetic excitation in-flight in the secondary target is one of the most important ingredients of the experiment, ideally adapted to the kinematic properties and to the low intensities of the secondary beams. It populates states in the vicinity of the fission barrier with large cross section of a few barns. Although the excitation energy acquired is not precisely known for a single event, the excitation-energy distribution can be calculated with rather good precision. The electromagnetic field of a lead target nucleus, seen by the projectile, can be represented by a flux of equivalent photons of different energies and multiplicities according to ref. (6). The projectiles are excited according to the energy-dependent photo absorption cross section which is dominated by the giant dipole resonance with small contributions of the giant quadrupole resonances. First-chance fission represents the main source of fission, but also fission after evaporation of one or two particles (mostly neutrons) occurs with a probability of about 20%. This leads to a reduction of the excitation energy at fission. The excitation-

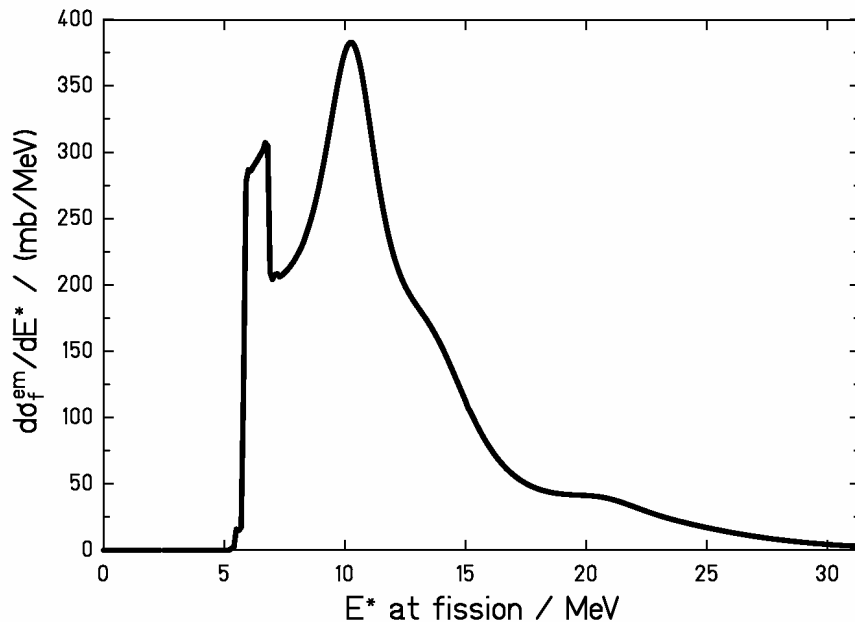


Figure 3. Calculated distribution of excitation-energies at fission after electromagnetic excitation of ^{234}U projectiles at 430 A MeV in a lead target.

energy distribution at fission after electromagnetic excitation of ^{234}U in the passage of a lead target at 430 A MeV is shown in Figure 3. For details of the calculation see ref.(4).

The calculated excitation-energy distributions of the other nuclei investigated are similar.

RESULTS AND DISCUSSION

In the present experiment, the elemental yields and the total kinetic energies of long isotopic chains from ^{205}At to ^{234}U have been determined. The elemental yields are shown in Figure 4 and Figure 5. The transition from symmetric fission in the lighter systems to asymmetric fission in the heavier systems is systematically covered. In the transitional region, around ^{226}Th , triple-humped distributions appear, revealing comparable intensities for symmetric and asymmetric fission. In particular for uranium and thorium isotopes strong even-odd effects are observed.

Fission channels

Turkevich and Niday (7) already noticed that different components which they named fission modes appear in the fission-fragment yields and in the kinetic-energy

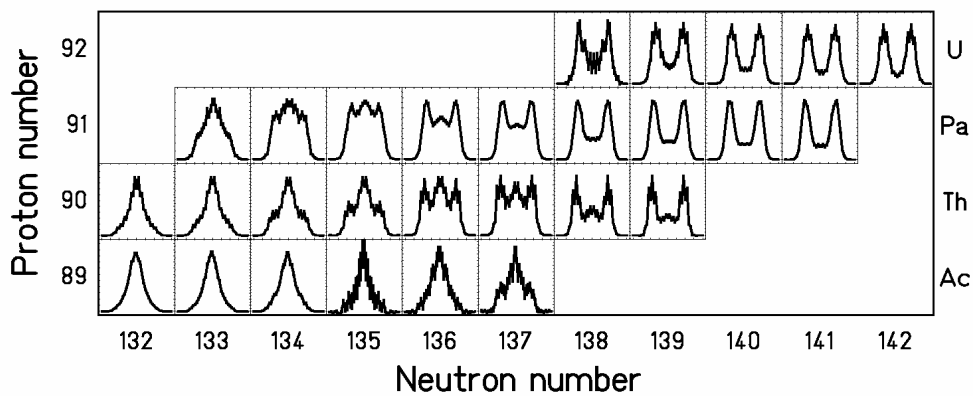


Figure 4. Measured fission-fragment charge distributions from ^{221}Ac to ^{234}U are shown on a chart of the nuclides.

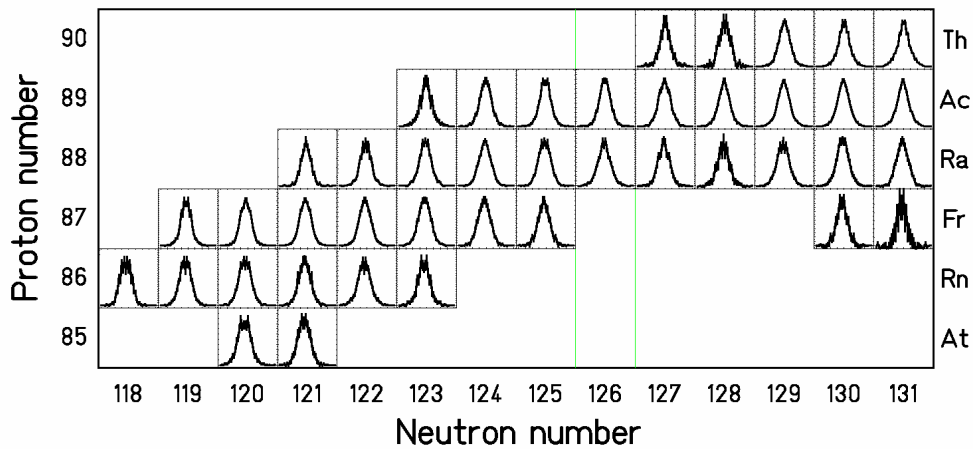


Figure 5. Measured fission-fragment charge distributions from ^{205}At to ^{221}Th are shown on a chart of the nuclides.

distributions. Later, models were proposed to deduce the fission characteristics from the properties of the scission configuration alone, e.g. ref. (8). However, these neglect the dynamic evolution of the system from saddle to scission which seems to be very important (9,10,11). The concept of independent fission channels has been developed (12,13) according to which the fissioning system follows specific valleys in the potential energy in the direction of elongation. Several properties (e.g. average mass or charge split, mass or charge width, mean total kinetic energy) could be related to calculated properties of the highly deformed fissioning system. However, the mechanisms which determine the fission-fragment yields are not sufficiently well understood to allow for quantitative predictions. Therefore, the intensities of the fission channels are usually deduced from experiment. The systematic survey on fissioning systems with strongly varying charge distributions (see Figure 4 and Figure 5) will provide a new test case for the concept of independent fission channels. Moreover, it will enable a more systematic view on how the intensities of the fission channels vary as a function of the nuclear composition.

At first glance, two fission components appear in the measured charge distributions, a symmetric and an asymmetric one. The weights of these two fission components were quantitatively determined by fitting three Gaussian curves to the charge-yield distributions. The widths (standard deviation) of the symmetric and the asymmetric components were found to be close to 4.0 charge units and 2.2 charge units, respectively, for all nuclei for which they could be extracted. In cases where either one of the components was too weak, the corresponding value from this systematics was imposed to the fit. The ratio of symmetric to asymmetric fission was then determined by the ratio of the areas of the Gaussians describing the data. The result of this procedure is shown in Figure 6. The transition is rather smooth, and the weights of the two fission components scale with the mass of the fissioning nucleus.

In detail, the charge-yield distributions and the total kinetic energies of ^{233}U , ^{232}Pa , ^{228}Pa , ^{228}Th , ^{226}Th , and ^{223}Th are shown in Figure 7. The gross structural effects observed in the charge yields are different from those showing up in the total kinetic energies. From ^{233}U to ^{223}Th , the weight of the asymmetric fission component decreases strongly, while the enhancement of the total kinetic energies near $Z = 52$ to 54 is preserved. In a simultaneous fit to elemental yields and total kinetic energies, it was possible to reproduce these data with the assumption of independent fission channels. A description with two fission channels only, which well reproduces the nuclear-charge yields, represents the measured *TKE* values only poorly. A satisfactory description was obtained with three channels, “standard I” at $N = 82$, “standard II” around $N = 88$ in the heavy fragment, and “superlong” at symmetry, using the notations introduced by Brosa et al. (13). Each channel was represented by a Gaussian distribution in the yields and a specific scission-point configuration. In order to consider the trivial variation of the total kinetic energy as a function of mass and charge split, the Coulomb repulsion V_C in the scission-point configuration was parametrized by the following expression, introduced in ref. (8):

$$V_C = \frac{Z_1 \cdot Z_2 \cdot e^2}{r_0 \left(A_1^{1/3} \cdot \left[1 + \frac{2\beta_1}{3} \right] + A_2^{1/3} \cdot \left[1 + \frac{2\beta_2}{3} \right] \right) + d} \quad (1)$$

Z_i , A_i and β_i are nuclear-charge numbers, mass numbers and deformations of the fission fragments, $r_0 = 1.16$ fm is the nuclear-radius constant, and e the elementary charge. The mass numbers were related to the charge numbers by the UCD assumption. The deformation parameters were fixed at $\beta_i = 0.6$ as predicted by the liquid-drop model, see ref. (8). The “tip distance” d was determined from a fitting procedure, requiring that the measured TKE values are best reproduced by V_C . Since the fit can only yield one parameter of equation (1), the elongation of the system, parametrized by the tip distance d , also effectively represents variations in the deformation of the fragments.

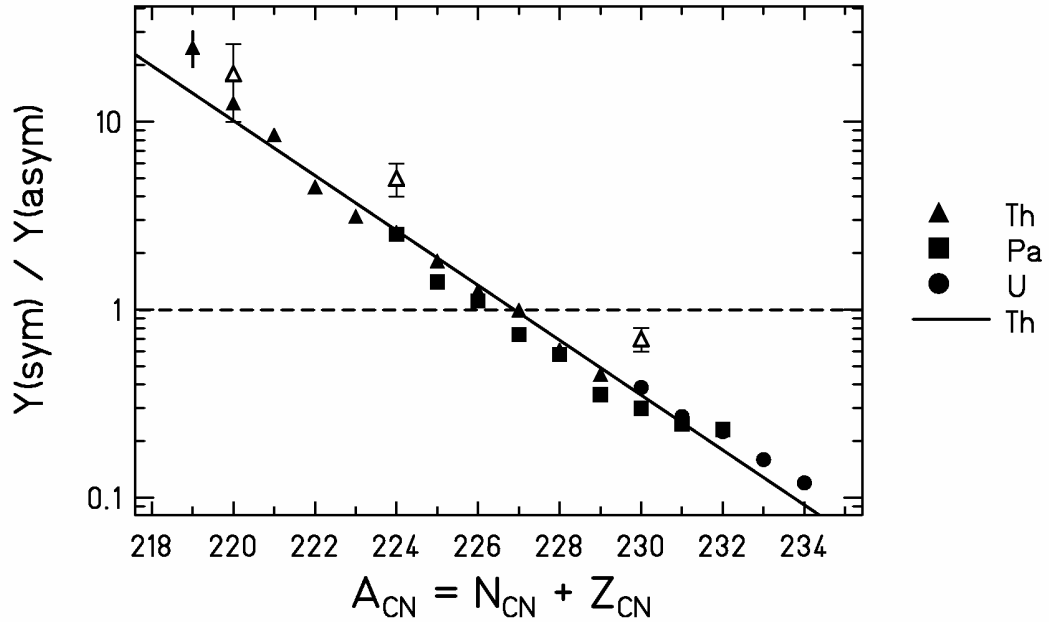


Figure 6. Intensity ratios of the symmetric and the asymmetric fission components in the transitional region as a function of mass number. The full triangles (squares, circles) correspond to thorium (protactinium, uranium) isotopes. The open symbols for ^{220}Th and ^{224}Th measured by Itkis et al. (14) and for ^{230}Th measured by Unik et al. (15) at somewhat higher excitation energies are included.

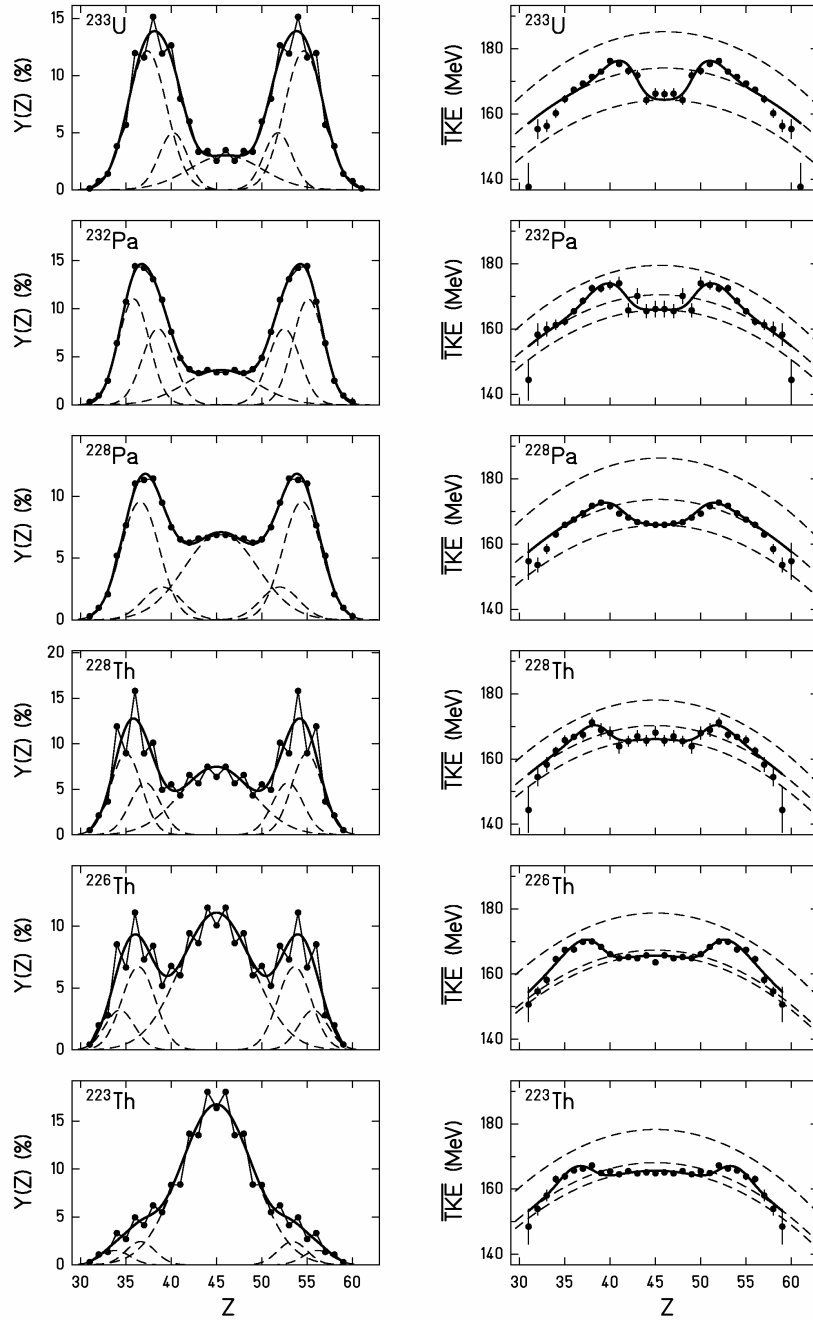


Figure 7. Measured elemental yields (left part) and average total kinetic energies (right part) as a function of the nuclear charge measured for fission fragments of several fissioning nuclei. Only statistical errors are given. The total kinetic energies are subject to an additional systematic uncertainty of 2 %, common to all data (5). Arrows indicate the positions of neutron ($N = 50, 82$) and proton shells ($Z = 50$). The positions of the neutron shells are calculated from the proton numbers by assuming an unchanged charge density (UCD). The full lines show descriptions with the model of independent fission channels. The contributions of the individual channels are depicted by dashed lines. (See text for details.)

Table 1. Parameters of the independent fission channels deduced from the data.

Nucleus	Channel	d / fm	Position	Width	Intensity
^{234}U	Standard I	0.88 (0.25)	52.7 (0.6)	2.13 (0.22)	49.7 (20.6)
	Standard II	2.06 (0.47)	55.2 (0.5)	2.07 (0.14)	39.1 (20.1)
	Superlong	2.83 (0.32)	46	4.0	11.2 (1.1)
^{233}U	Standard I	0.59 (0.21)	51.8 (0.2)	1.57 (0.12)	20.0 (5.5)
	Standard II	1.63 (0.06)	54.6 (0.2)	2.14 (0.06)	66.2 (5.4)
	Superlong	2.68 (0.13)	46	4.0	13.8 (0.5)
$^{232}\text{U}^*$	Standard I	0.85 (0.15)	52.4 (0.2)	1.91 (0.07)	35.2 (3.4)
	Standard II	1.69 (0.10)	55.1 (0.2)	1.91 (0.07)	46.9 (3.9)
	Superlong	2.19 (0.18)	46	4.0	17.9 (0.8)
^{232}Pa	Standard I	0.77 (0.16)	52.5 (0.4)	1.75 (0.17)	34.9 (9.8)
	Standard II	1.64 (0.13)	55.1 (0.2)	1.70 (0.08)	47.0 (9.6)
	Superlong	2.13 (0.16)	45.5	4.0	18.1 (0.8)
$^{231}\text{Pa}^*$	Standard I	0.74 (0.10)	52.5 (0.1)	1.85 (0.04)	31.8 (2.5)
	Standard II	1.54 (0.05)	55.0 (0.1)	1.85 (0.04)	48.8 (2.7)
	Superlong	2.24 (0.09)	45.5	4.0	19.4 (0.4)
$^{230}\text{Pa}^*$	Standard I	0.35 (0.20)	52.6 (0.2)	1.95 (0.05)	26.9 (4.3)
	Standard II	1.60 (0.08)	54.9 (0.1)	1.95 (0.05)	50.6 (4.5)
	Superlong	2.29 (0.09)	45.5	4.0	22.5 (0.5)
$^{229}\text{Pa}^*$	Standard I	0.45 (0.13)	52.5 (0.1)	1.87 (0.05)	27.6 (2.8)
	Standard II	1.57 (0.07)	54.9 (0.1)	1.87 (0.05)	47.0 (3.0)
	Superlong	2.38 (0.08)	45.5	4.0	25.4 (0.5)
$^{228}\text{Pa}^*$	Standard I	0.25 (0.30)	52.0 (0.3)	2.11 (0.04)	13.8 (4.0)
	Standard II	1.42 (0.06)	54.4 (0.1)	2.11 (0.04)	50.7 (4.2)
	Superlong	2.23 (0.05)	45.5	4.0	35.5 (0.4)
$^{228}\text{Th}^*$	Standard I	0.63 (0.24)	52.9 (0.3)	1.70 (0.09)	24.4 (5.7)
	Standard II	1.38 (0.12)	55.0 (0.2)	1.70 (0.09)	38.1 (6.0)
	Superlong	1.81 (0.10)	45	4.0	37.5 (1.0)
^{226}Th	Standard I	0.62 (0.10)	53.6 (0.3)	1.85 (0.13)	31.2 (7.4)
	Standard II	1.72 (0.52)	55.7 (0.3)	1.63 (0.10)	13.2 (7.3)
	Superlong	1.90 (0.03)	45	4.0	55.6 (0.4)
^{225}Th	Standard I	0.82 (0.12)	53.8 (0.2)	1.85 (0.08)	25.4 (3.4)
	Standard II	2.44 (0.50)	56.1 (0.5)	1.82 (0.15)	6.0 (3.3)
	Superlong	2.01 (0.02)	45	4.0	68.6 (0.4)
^{224}Th	Standard I	0.18 (0.47)	52.8 (0.3)	1.51 (0.16)	6.3 (3.2)
	Standard II	1.48 (0.10)	55.0 (0.3)	1.93 (0.09)	17.9 (3.2)
	Superlong	1.98 (0.02)	45	4.0	75.8 (0.4)
$^{223}\text{Th}^*$	Standard I	0.72 (0.11)	53.4 (0.1)	1.61 (0.06)	9.9 (0.4)
	Standard II	1.71 (0.15)	56.2 (0.1)	1.61 (0.06)	6.1 (0.4)
	Superlong	1.98 (0.02)	45	4.0	84.0 (0.4)
$^{222}\text{Th}^*$	Standard I	0.85 (0.20)	53.3 (0.2)	1.65 (0.11)	6.6 (0.6)
	Standard II	1.64 (0.19)	56.0 (0.2)	1.65 (0.11)	5.2 (0.7)
	Superlong	1.97 (0.02)	45	4.0	88.2 (0.6)
^{223}Ac	Standard I	0.85 (0.35)	52.2 (0.2)	0.84 (0.30)	3.8 (2.6)
	Standard II	0.90 (0.22)	54.5 (0.7)	1.89 (0.40)	7.8 (2.6)
	Superlong	1.65 (0.03)	44.5	4.0	88.4 (1.2)

The positions are given in Z for the heavy group. The width corresponds to the standard deviation. The width of the superlong channel was fixed to 4.0 charge units from the systematics described above.

*) For these nuclei the widths of standard I and standard II were set equal in the fit.

For each fission channel, position, width, and height of the Gaussian representing the nuclear-charge yields as well as the tip distance of the scission configuration were treated as free parameters. The width of the superlong channel had to be kept constant for the fit to converge. The yields are formulated as the sum, the total kinetic energies as the weighted average of the different components. The results are given in table 1. Unfortunately, the dispersion of the total kinetic energy could not be deduced in the secondary-beam experiment due to the limited resolution. Therefore, the relative weights of the two asymmetric fission channels could only be determined with rather large error bars.

The parameters, in particular the relative heights of the total kinetic energies, attributed to the individual fission channels, roughly coincide with the expectations from systematics of the three most intense fission channels known from heavier fissioning systems (16,17,18,19,20,21). Also for thorium isotopes produced at higher excitation energies by fusion reactions and for nuclei in the lead region, standard I and standard II fission channels have been observed (14,22,23). As a remarkable result, we found that the superlong channel which appears at symmetry becomes more compact for the lighter systems. This finding indicates that this channel is influenced by shell effects, too, although the charge distribution can be represented by a simple Gaussian. The variation of the tip distance in the symmetric channel can be related to the properties of the shell around $N = 64$ which tends to become less deformed with decreasing neutron number (see e. g. refs. 8,24). Moreover, the symmetric channel appears to be much narrower than observed previously in heavier systems.

From the good simultaneous description of nuclear-charge yields and total kinetic energies as demonstrated by Figure 7 we conclude that the concept of independent fission channels has passed an important test. It allows for the strong variations of the yields while keeping the *TKE* distributions almost unchanged. However, we would also like to add a critical remark. In accordance with the usual treatment, the most probable scission-point configuration, parametrized by the tip distance d , was fixed at one value for each fission channel and not allowed to vary as a function of charge split. This might be a severe oversimplification. It is known that the energetically most favourable deformation in a deformed shell region varies with the number of nucleons (8,24). Therefore a corresponding variation of the mean elongation at the scission point as a function of the charge split is to be expected. This would imply a variation of the most probable tip distance d even inside one fission channel. Besides the symmetric channel, this also concerns the standard II fission channel related to the $N = 88$ deformed shell. Therefore, part of the increase of the *TKE* values in the asymmetric component towards symmetry, which is attributed to the compact standard I channel in our description, may rather be imputed to a variation of the scission configuration in the standard II channel to more compact shapes. This would strongly affect all parameters of the two asymmetric fission channels.

The data on elemental yields support the idea, stated by Itkis et al. (22), that the weights of the fission channels are principally determined by an interplay of the neutron shells at $N = 82$ and $N = 86$ with the liquid-drop potential. A quantitative description of this idea has been formulated by J. Benlliure et al. (25) by relating the charge distributions to the density of transition states in the vicinity of the outer fission barrier. The total kinetic energies, however, seem to be closely related to the ground-state properties of the fission fragments. This finding agrees with the expectation that the

total kinetic energies are essentially determined by the shell effects in the scission-point configuration.

Dissipation in fission

Data on even-odd effects in elemental yields were difficult to obtain in conventional fission experiments. The rather scarce data on total even-odd effects measured previously show a systematic variation with the fissility of the fissioning system (see Figure 8). From this variation, the intrinsic excitation energy acquired by dissipation up to scission was deduced to grow with increasing fissility (26). The excellent nuclear-charge resolution of the present experiment allowed to determine the even-odd structure in the elemental yields for a large number of fissioning systems. The new results on total even-odd effects for thorium and uranium isotopes of the present work which are also shown in Figure 8 seem to be compatible with the previously measured data: The higher excitation energies present in electromagnetic-induced fission (see Figure 3) lead to a reduction by about 40 % , but the dependence on the fissility parameter Z^2/A observed previously is confirmed.

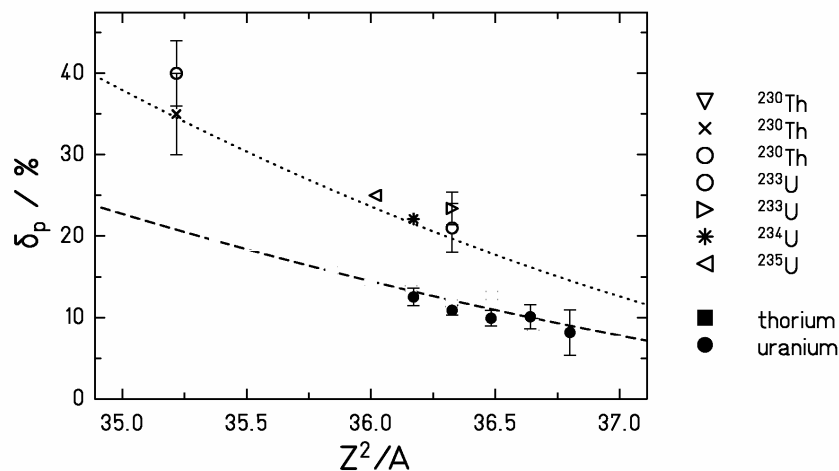


Figure 8. Total even-odd effect in the nuclear-charge yields observed in the fission of different nuclei. Data from thermal-neutron-induced fission (open symbols) from literature are compared to results of the present experiment for thorium and uranium isotopes (full symbols) as a function of the fissility parameter Z^2 / A .

However, in the secondary-beam experiment, strong local even-odd structures have also been found (27) for all investigated odd- Z fissioning systems. A similar observation for a few other odd- Z systems is reported by Denschlag et al. (28). We attributed these findings to an enhanced sticking probability of unpaired protons to the heavy fragment due to phase-space arguments in asymmetric charge splits (27). This implies that an enhanced production of fission products with even proton numbers cannot directly be related to the probability of a fully paired proton configuration to survive up to the scission point as was done before (29). Only for symmetric charge splits, the analysis used so far is valid. For asymmetric charge splits, however, part of the measured even-odd structure has to be attributed to the statistical contribution.

The present experiment for the first time provides data on even-odd structure in symmetric charge splits for long isotopic chains. Figure 9 shows the local proton even-odd effect as defined by Tracy et al. (30) for thorium isotopes both at symmetry and in the maximum of the asymmetric fission component. From this figure, we get a completely different impression than from Figure 8: The local even-odd effect at symmetry which is directly related to the intrinsic excitation energy at scission remains constant over nine isotopes. From this we conclude that the intrinsic excitation energy at the scission point is the same for all thorium isotopes investigated. The local even-odd effect at asymmetry is much larger, probably due to the statistical contribution, and it is also almost constant. We understand now the true reason for the strong variation of the even-odd effect for thorium isotopes (and also for uranium isotopes): It is the strong variation of the relative weights of symmetric and asymmetric components in the fission yields, see Figure 6. With increasing neutron number (decreasing fissility), the relative weight of the asymmetric component grows, leading to a larger total even-odd effect.

Let us now consider the global even-odd effects found for thermal-neutron-induced

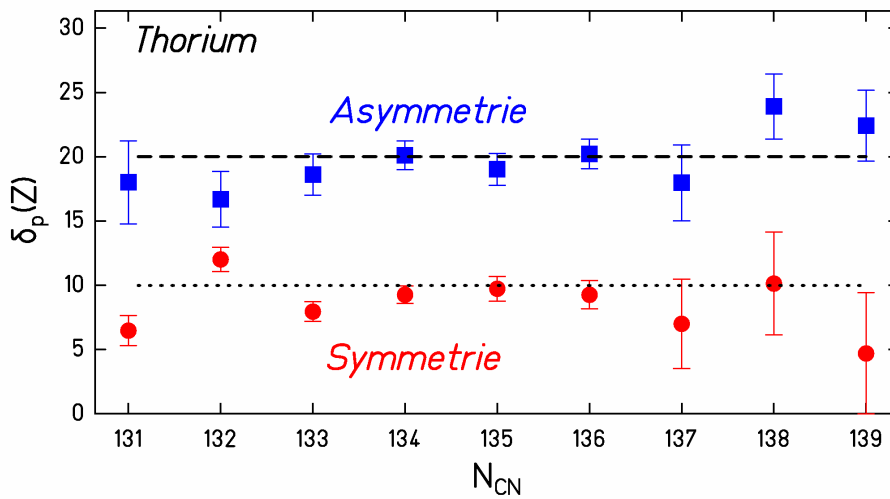


Figure 9. Local even-odd effect for symmetric and the most abundant asymmetric charge splits found in the fission of thorium isotopes after electromagnetic excitation.

fission of the heavier systems shown in Figure 8. According to our new understanding, great part of the measured total even-odd structure must be attributed to the statistical contribution. Here, symmetric fission is too weak to play any role. In these cases, another effect is expected to account for a great part of the observed variation of the total even-odd effect: Due to the constant position of the heavy fission peak in mass number, the light and heavy peak come closer to each other with increasing mass of the fissioning system. Thus, the average asymmetry and consequently the statistical contribution to the even-odd structure decreases. Due to the restricted range of A/Z values, increasing mass goes in line with increasing fissility.

We have shown that the interpretation of the measured even-odd effect in terms of energy dissipation in fission is much more complex than thought up to now. It is presently not clear whether the observed variations of the even-odd structure for different fissioning systems can fully be explained by a variation of the statistical contribution. A final answer on this question would require a far more detailed analysis

and a full quantitative understanding of the statistical contribution to the even-odd structure in fission, including the influence of shell structure.

CONCLUSION

A new experimental technique was applied to measure elemental yields and total kinetic energies after low-energy fission of short-lived radioactive nuclei. The beautiful data nicely demonstrate the decisive influence of nuclear structure on the fission process in a particular interesting transitional region around ^{227}Th . In contrast to the total kinetic energies, the element distributions were found to vary strongly, essentially as a function of mass number of the fissioning system. This behaviour could well be reproduced by the model of independent fission channels. The weights of the asymmetric fission channels decrease with decreasing mass of the fissioning nucleus, but the scission-point configurations remain unchanged. The scission-point configuration of the symmetric fission channel, however, evolves to more compact shapes for the lighter fissioning nuclei, where symmetric splits correspond to smaller nucleon numbers. This clearly reveals the influence of shell effects also in the symmetric channel.

The new understanding of the even-odd effect in fission deduced from the present data requires a revised interpretation of even-odd effects in fission. Strong variations of the observed even-odd effect in the elemental yields for different systems and as a function of asymmetry for a specific system are attributed to a great part to a statistical contribution to this quantity rather than to a variation of the intrinsic excitation energy at scission. Conclusions on the viscosity of cold nuclear matter have to be reconsidered.

REFERENCES

1. H.-G. Clerc, M. deJong, T. Brohm, M. Dornik, A. Grewe, E. Hanelt, A. Heinz, A. R. Junghans, C. Röhl, S. Steinhäuser, B. Voss, C. Ziegler, K.-H. Schmidt, S. Czajkowski, H. Geissel, H. Irnich, A. Magel, G. Münzenberg, F. Nickel, A. Piechacyek, C. Scheidenberger, W. Schwab, K. Sümmerer, W. Trinder, M. Pfützner, B. Blank, A. Ignatyuk, G. Kudyaev, Nucl. Phys. **A590** (1995) 785
2. A. R. Junghans, M. de Jong, H.-G. Clerc, A. V. Ignatyuk, G. A. Kudyaev, K.-H. Schmidt, Nucl. Phys. **A629** (1998) 635
3. H. Geissel, P. Armbruster, K.-H. Behr, A. Brünle, K. Burkard, M. Chen, H. Folger, B. Franczak, H. Keller, O. Klepper, B. Langenbeck, F. Nickel, F. Pfeng, M. Pfützner, E. Roeckl, K. Rykaczewski, I. Schall, D. Schardt, C. Scheidenberger, K.-H. Schmidt, A. Schröter, T. Schwab, K. Sümmerer, M. Weber, G. Münzenberg, T. Brohm, H.-G. Clerc, M. Fauerbach, J.-J. Gaimard, A. Grewe, E. Hanelt, B. Knödler, M. Steiner, B. Voss, J. Weckenmann, C. Ziegler, A. Magel, H. Wollnik, J.P. Dufour, Y. Fujita, D. J. Vieira, B. Sherrill, Nucl. Instr. Meth. **B70** (1992) 286
4. A. Grewe, S. Andriamonje, C. Böckstiegel, T. Brohm, H.-G. Clerc, S. Czajkowski, E. Hanelt, A. Heinz, M. G. Itkis, M. de Jong, M. S. Pravikoff, K.-H. Schmidt, W. Schwab, S. Steinhäuser, K. Sümmerer, B. Voss, Nucl. Phys. **A614** (1997) 400
5. C. Böckstiegel, S. Steinhäuser, J. Benlliure, H.-G. Clerc, A. Grewe, A. Heinz, M. de Jong, A. R. Junghans, J. Müller, K.-H. Schmidt, Phys. Lett. **B398** (1997) 259
6. B. Baur, C. A. Bertulani, Phys. Rev. **C34** (1986) 1654
7. A. Turkevich, J. B. Niday, Phys. Rev. **84** (1951) 52
8. B. D. Wilkins, E. P. Steinberg, R. R. Chasman, Phys. Rev. **C14** (1976) 1832
9. P. Möller, S. G. Nilsson, Phys. Lett. **31B** (1970) 283
10. G. A. Kudyaev, Yu. B. Ostapenko, G. N. Smirenkin, Sov. J. Nucl. Phys. **45** (1987) 951
11. H. Kudo, H. Muramatsu, H. Nakahara, K. Miyano, I. Kohno, Phys. Rev. **C25** (1982) 3011
12. V. V. Pashkevich, Nucl. Phys. **A169** (1971) 275

-
13. U. Brosa, S. Grossmann, A. Müller, Phys. Rep. **197** (1990) 167
 14. M. G. Itkis, Yu. Ts. Oganessian, G. Chubarian, V. N. Okolovich, G. N. Smirenkin, in Nuclear Fission and Fission-product Spectroscopy, H. Faust and G. Fioni (eds.), ILL Grenoble (1994) pp. 77
 15. J. P. Unik, J. R. Huizenga, Phys. Rev. **B134** (1964) 90
 16. H. H. Knitter, F.-J. Hambsch, C. Budtz-Jorgenson, J. P. Theobald, Z. Naturforsch. **42a** (1987) 786
 17. P. Schillebeeckx, C. Wagemans, A. J. Deruytter, R. Barthélémy, Nucl. Phys. **A545** (1992) 623
 18. S. Pommé, E. Jacobs, M. Pissens, D. De Frenne, K. Persyn, K. Govaert, M. L. Yoneama, Nucl. Phys. **A572** (1994) 237
 19. P. Schillebeeckx, C. Wagemans, P. Geltenbort, F. Gönnerwein, A. Oed, Nucl. Phys. **A580** (1994) 15
 20. L. Demattè, C. Wagemans, R. Barthélémy, P. D'hondt, A. Deruytter, Nucl. Phys. **A617** (1997) 331
 21. C. Donzaud, S. Czajkowski, P. Armbruster, M. Bernas, C. Böckstiegel, Ph. Dessange, H. Geissel, E. Hanelt, A. Heinz, C. Kozhuharov, Ch. Miehé, G. Münzenberg, M. Pfützner, W. Schwab, C. Stéphan, K. Sümmerer, L. Tassan-Got, B. Voss, Europh. J. **A1** (1998) 407
 22. M. G. Itkis, V. N. Okolovich, A. Yu. Rusanov, G. N. Smirenkin, Sov. J. Part. Nucl. **19** (1988) 301
 23. S. D. Beizin, S. V. Zhdanov, M. G. Itkis, V. N. Okolovich, G. N. Smirenkin, Sov. J. Nucl. Phys. **53** (1991) 411
 24. I. Ragnarsson, R. K. Sheline, Physica Scripta **29** (1984) 385
 25. J. Benlliure, A. Grewe, M. de Jong, K.-H. Schmidt, S. Zhdanov, Nucl. Phys. **A628** (1997) 458
 26. F. Gönnerwein, "The Nuclear Fission Process", CRC Press, London, 1991, C. Wagemans ed., pp. 409
 27. S. Steinhäuser, J. Benlliure, C. Böckstiegel, H.-G. Clerc, A. Heinz, A. Grewe, M. de Jong, A. R. Junghans, J. Müller, M. Pfützner, K.-H. Schmidt, Nucl. Phys. **A634** (1998) 89
 28. H. O. Denschlag et al., contribution to this workshop
 29. H. Nifenecker, G. Mariolopoulos, J. P. Bocquet, R. Brissot, Mme Ch. Hamelin, J. Crancon, Ch. Ristori, Z. Phys. **A308** (1982) 39
 30. B. L. Tracy, J. Chaumont, R. Klapisch, J. M. Nitschke, A. M. Poskanzer, E. Roeckl, C. Thibault, Phys. Rev. **C5** (1972) 222